Mon. Not. R. astr. Soc. (1980) **192**, 209–232

Correlation analyses of deep galaxy samples – II. Wide angle surveys at the South Galactic Pole

T. Shanks, R. Fong and R. S. Ellis *Department of Physics, Durham University*

H. T. MacGillivray *Royal Observatory, Edinburgh*

Received 1979 December 7; in original form 1979 August 16

Summary. Angular correlation functions are presented for samples of galaxies found by measurement of five Schmidt plates with the COSMOS machine. The plates include J–R pairs of two fields and have been limited at various magnitudes down to $J = 21.5$ and $R = 19.75$. On small angular scales ($< 0.3^\circ$) the amplitudes of the correlation functions are in reasonable agreement with those expected from the scaling of local results, indicating the uniformity and isotropy of the Universe to very great depths ($\sim 700\ h^{-1}$ Mpc). However, the errors are still too large to put useful constraints on evolution in galaxy clustering. At large angular scales ($> 0.3^\circ$) we find convincing evidence for a feature in the correlations similar to that discovered by Groth & Peebles in the correlation analysis of the Lick catalogue. Its position corresponds to a physical separation of $3\ h^{-1}$ Mpc, some three times smaller than that of Groth & Peebles.

1 Introduction

In the first paper in this series (Phillipps *et al.* 1978; hereafter Paper I) we showed how it was possible to compare angular covariance functions for galaxies on deep ($\lesssim$ 22nd magnitude) surveys with those measured locally. Such comparisons test the applicability of a single model of galaxy clustering over large volumes of space. With sufficient precision and a good knowledge of the properties of normal galaxies, it might also be possible to place observational constraints on the dynamical evolution of galaxy clustering over the look-back time implied by the deep samples, (see Fall 1979, for a review of work on galaxy correlations and their relevance to cosmology).

In Paper I we applied the technique to a sample of about 3000 galaxies contained in machine-measured scans of a 2 deg^2 region of a J–R plate pair of the same Schmidt field. Comparisons with local samples revealed a puzzling discrepancy of ~ 2.5 in both passbands, in the sense that the deep samples appeared to be less clustered (after allowance had been made for projection). The selection effects operating on deep samples were considered by Ellis, Fong & Phillipps (1977; hereafter EFP). The uncertainty in these criteria was thought

to be insufficient to resolve this discrepancy. It was concluded that sampling problems were the most likely explanation. Initially it was not known how large an area of sky would be required to make a deep sample 'fair' for this purpose. Here we repeat the analyses on five samples, *each* with an area ≈ 7 times larger than in Paper I.

With the increase in sample size, it is now also possible to check the reproducibility of the feature at large angle found by Groth & Peebles (1977) in their analysis of the Shane–Wirtanen (SW) counts. This feature is important for theories of galaxy formation as it marks the transitional region between the linear and non-linear regimes of galaxy clustering in the gravitational instability picture (Davis, Groth & Peebles 1977; Efstathiou 1979). In this context its existence and position can be used as a cosmological test.

An outline of the paper follows. In Section 2 we discuss the photographic material and the measurement procedure. We have modified the star–galaxy separation algorithm since Paper I and determine a photometric scale from a comparison of measured quantities with stellar sequences and galaxy isophotometry. In Section 3 we describe the methods we use for estimating the angular covariance function. Section 4 summarizes the scaling procedure and Section 5 examines the results on small angular scales ($\lesssim 15$ arcmin), where the correlations are large and expected to follow a power-law in separation of index ~ -0.8. We also compare the correlation amplitudes with those obtained in shallower surveys. In Section 6 we study the large scale correlations, where the clustering is weak. We discuss the evidence for a feature in the correlation function and compare our results with those of Groth & Peebles. Section 7 lists our conclusions.

2 Data

2.1 PHOTOGRAPHIC MATERIAL AND ITS MACHINE MEASUREMENT

The material consists of five plates taken with the 1.2-m UK Schmidt telescope (UKST). The plates constitute two adjacent J–R pairs plus a further adjacent J plate in the region of the South Galactic Pole (SGP). Details are given in Table 1. The plates were taken during good seeing conditions and are representative of the very high quality photography possible with this telescope.

The central unvignetted areas of these plates (≈ 14 deg^2) were scanned in various ways by the COSMOS measuring machine at the Royal Observatory, Edinburgh (Pratt *et al.* 1975).

Table 1. Photographic material.

Field	RA	Dec	UKST no.	Date	Exposure	Effective seeing (arcsec)
SGP	$0^h\,53^m$	$-28°\,03$	J3721	Nov. 4 1977	80 min	3.25
			R2775	Dec. 19 1976	90 min	3.5
SRC 412	$01^h\,09^m$	$-30°\,00$	J1920	Nov. 25 1975	60 min	3.25
			R3780	Dec. 1977	90 min	3.25
SRC 475	$01^h\,06^m$	$-25°\,00$	J1916	Nov. 25 1975	60 min	3.5

Notes:

J = Kodak IIIa-J plus Schott GG 395.
R = Kodak IIIa-F plus Schott RG 630.
(In Paper I the Kodak 098 emulsion was used.)
Coordinates are plate centres for 1950.0 epoch.
The effective seeing is defined as the diameter of a faint star (after convolution with the COSMOS spot) within which 90 per cent of the intensity of the star image falls.

Table 2. The data.

Plate no.	Sky brightness (mag arcsec^{-2})	Threshold (per cent of sky)	Area scanned (deg^2)	Area drilled	Number density Galaxies (deg^{-2})	Stars
J3721	23.0	9	14.25	1.07	1311	1463
R2775	21.75	7	14.15	1.14	1105	999
J1920	22.5	7	14.88	0.44	1553	1338
R3780	21.75	7	13.61	1.63	1361	1016
J1916	22.5	7	13.35	1.97	1571	1592

Notes:

The threshold values are based on COSMOS measurements of the north calibration wedges on UKST plates.
The number densities refer to those to limiting magnitudes $J = 21.5$ and $R = 19.75$.
The area drilled refers to portions of the data removed because of detection problems around bright stars.

In addition to the Coarse Mode (CM) of measurement described in EFP we have also used Mapping Mode (MM) where each 16 μm ($\approx$ 1.1 arcsec) pixel transmission is recorded. In this manner COSMOS acts as a very fast microdensitometer. The MM scans were used to check the CM algorithms using software developed by MacGillivray (see MacGillivray & Dodd 1979). However, most of the analysis in this paper will use the CM runs.

To allow the extension of our analyses to larger areas certain changes have been made to the CM procedures used in Paper I. First, the background following algorithm can now deal more reliably with changes in the emulsion sensitivity across the plate. The background intensity contours measured by COSMOS correspond well with variations found on the plates using the high contrast printing technique developed by Malin (1978). Secondly, to improve photometric accuracy, measurements were made to lower surface brightness thresholds; here these thresholds were usually set at 7 per cent of the sky brightness (see Table 2), whereas in Paper I 15 per cent were used. Thirdly, although images as small as 10 pixels were recorded, care was taken to define our sample limits sufficiently bright so that not more than a few per cent of the sample had less than 50 measured 8-μm (0.54 arcsec) pixels. This improves the photometric accuracy at the faint limits of our samples.

2.2 STAR–GALAXY SEPARATION

The most difficult aspect of Schmidt plate analysis is star–galaxy separation because, over the magnitude range 18–22, the surface density of stars exceeds that of galaxies. The basic method employed here follows that developed by MacGillivray *et al.* (1976) (see also Oemler 1974) which uses the lower surface brightness of galaxies as the distinguishing criterion. A typical plot of central surface brightness as represented by the minimum transmission, $T_{\min}$, and A, the measured number of pixels, for images classified by eye in a 1 cm^2 ($\approx$ 125 arcmin^2) area is shown in Fig. 1. The indicated star curve flattens out for bright images because of saturation. At the fainter end the flattening is due to the increasing proportion of sky measured within the total image intensities. Third-order polynomials were fitted to sections of the star curve as determined from one small area of the plate. The curves were translated to give the best upper envelope for the star distribution on the $T_{\min}$–A plot.

To apply these curves to large areas it is necessary to correct for changing background across the plate. This affects the star curve most at its fainter end and we adjust the upper

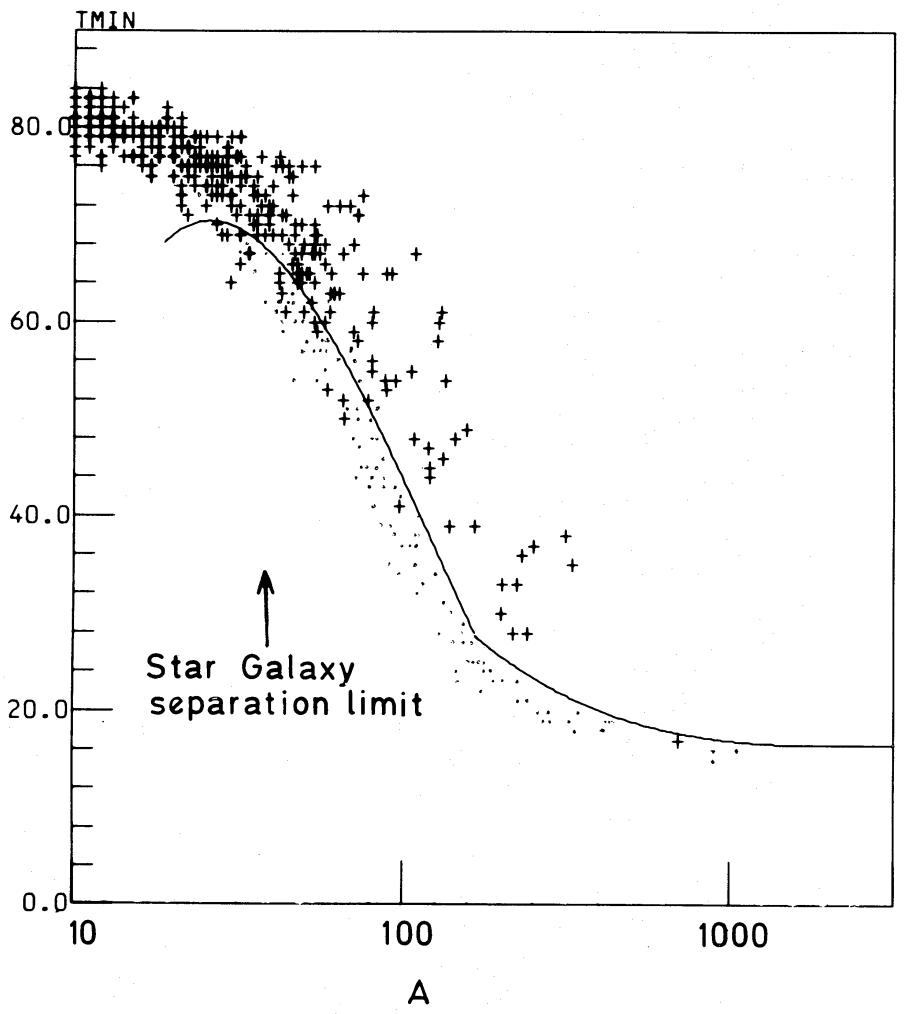

Figure 1. The distribution of minimum transmission, T_{min}, and isophotal area A for all images within a 1 cm² area of a J plate. Plus signs represent images classified by eye as galaxies; dots represent stars. The curve is the most successful set of cubics dividing the distribution with area $A \geqslant 50$ into the two types.

envelope according to the local background using a technique which will be fully described elsewhere (Fong, in preparation). A correction is also needed to allow for a slight defocusing of the COSMOS spot caused by sagging of the plate in the plateholder. This effective increase in the 'seeing' moves the actual division between stars and galaxies further to the right in Fig. 1 than otherwise would be predicted. To correct for this effect we fit Gaussian profiles to every image and the median 'seeing' is then determined for each square in a 5 x 5 grid covering the plate. A 'seeing' map is then formed by interpolation. The star–galaxy curve of Fig. 1 is then shifted along the $\log A$ axis by an amount $k\Delta S$ where k is a fitted constant for each plate and ΔS is the change in the median 'seeing'. The effect of defocusing on image detection was also checked. In experiments where the spot was gradually defocused it was found that detection was only affected for images much smaller than our 50 pixel limit.

Finally, visual checks were made at random by several observers to ensure that the envelopes were accurately classifying images. The algorithm works to >90 per cent efficiency for images above the 50 pixel limit. To check further how successful this automatic classification has been, we determined, as in Paper I, the correlation between

number-density and background transmission for stars and galaxies and found it showed no significant bias. Fig. 2 shows the distributions of images classified as stars and galaxies on plate J3721. The randomness of the star distribution as opposed to the clumpy galaxy distribution is further evidence for the success of the above methods.

2.3 PHOTOMETRIC SCALE

COSMOS CM does not provide integrated intensities and resort must be made to the slower MM data for isophotal or total magnitudes. With CM data it was found (Fong, in preparation; Shanks 1979a) that a Gaussian fitted to the central intensity above sky, I_0, and the threshold intensity, $I_t = I[r = (A/\pi)^{1/2}]$, followed closely the MM profile for faint stars and galaxies (see Fig. 3). The total magnitude relative to sky is then calculated by integrating the Gaussian fit.

These relative magnitudes can be made absolute by using either simultaneous night sky readings or by comparing with stellar or galaxy photometry. Unfortunately, the UKST night sky photometer is immovable and takes simultaneous readings at the South Celestial Pole introducing an unknown correction when transferring to the field concerned. We also have evidence for substantial variations in the night sky brightness at Siding Spring over the 2-yr period between the taking of plates J1916/1920 and that of plate J3721; small overlap regions show the sky for plates J1916/1920 to be 0.5 mag brighter than that for J3721. This makes it impossible to use any subsequent photometry of the sky brightness in these regions.

There are also difficulties with calibration using stellar sequences. The presence of a discernible 'halo' around the COSMOS spot causes an uncertain scale error in its photometric scale at the bright end, necessitating the use of only faint ($\gtrsim$ 19.5 mag) sequences which are rare in the southern skies. We have used two unpublished sequences in the SGP field, kindly provided by Drs M. R. S. Hawkins (Edinburgh) and J. Graham (Cerro Tololo). Comparisons with the relative magnitudes yield a sky brightness of $\mu_J^{sky} = 22.7 \pm 0.5$ mag arcsec^{-2} for J3721. We also have photometry of the spiral galaxy NGC 253 (Pence, private communication) which lies on the same plate. PDS measurements of this plate by Drs J. Godwin and D. Carter give $\mu_J^{sky} = 23.0 \pm 0.15$ mag arcsec^{-2}. Adopting this as the more accurately determined value, we obtain sky brightnesses for the other J plates using small overlapping regions (see Table 2). In the R band, we have only the sequences provided by Dr Hawkins. From these, we obtain a value $\mu_R^{sky} = 21.75$ mag arcsec^{-2}. Clearly the reliable calibration of these and, indeed, all southern plates requires more investigation and careful observation. Of course, our relative magnitudes are not affected by these uncertainties.

The resulting differential number–magnitude counts for these plates are given in Fig. 4. The counts are in good agreement, both in slope and zero point, with others available in this magnitude range. As some of these results e.g. Kron (1978) rest on careful absolute photometry, this gives a good consistency check on our photometric procedure.

3 The computation of the angular correlation function

3.1 ESTIMATORS

The estimation of the angular correlation function, $w(\theta)$, was done in two parts. For angular separation $\theta < 0.1^\circ$, we first computed the number of pairs of galaxies in bins of constant width $\Delta \log \theta$, excluding those galaxies which fell in drilled regions (see Paper I). The same number of points were then randomly distributed over an identically drilled area and the

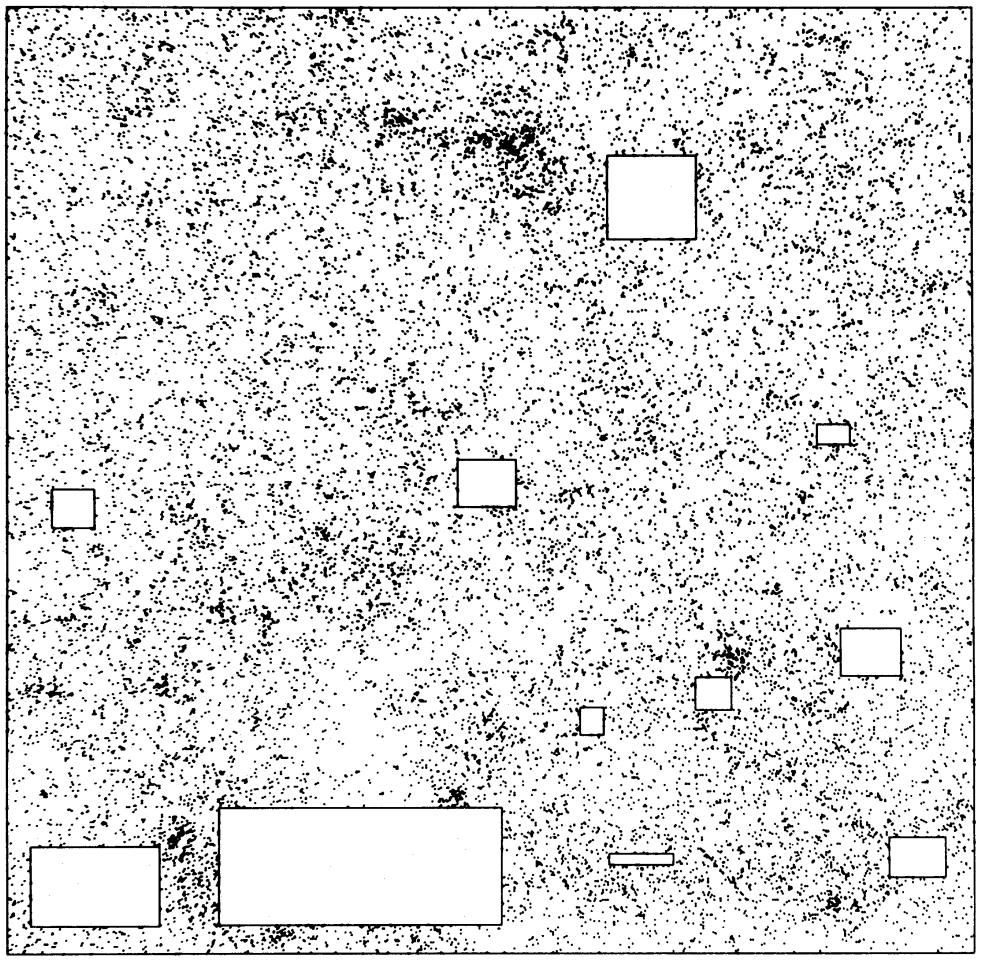

(a)

Figure 2. The distribution in position of images classified as (a) galaxies, and (b) stars, for the 3.8° × 3.8° sample limited at $J = 21.5$ on the plate J3721. The boxes represent areas 'drilled' out because they were occupied by bright stars around which the COSMOS detection routines are not expected to work consistently. The difference in clumpiness between the two distributions is evidence for the success of the star–galaxy separation alogorithm.

procedure repeated. The resulting estimator is

$$w(\theta) = N_d(\theta)/N_r(\theta) - 1 \quad (1)$$

where N_d is the number of actual pairs at separation θ and N_r the equivalent for the random distribution.

For larger angles, $\theta > 0.1^\circ$, the galaxies were first binned into 64 × 64 bins of size ~ 12 arcmin^2. Taking the galaxy separation as the distances between bin centres, the covariance function for this region was estimated using the relation

$$w(\theta) = N_p(\theta)/[N_b(\theta)\bar{n}] - 1 \quad (2)$$

where N_p is the total number of pairs computed in the separation range $(\theta - \Delta\theta/2, \theta + \Delta\theta/2)$, $N_b(\theta)$ is the number of bins used to find N_p and $\bar{n}$ is the average number of galaxies per bin. Any bin that overlapped a drilled region was excluded.

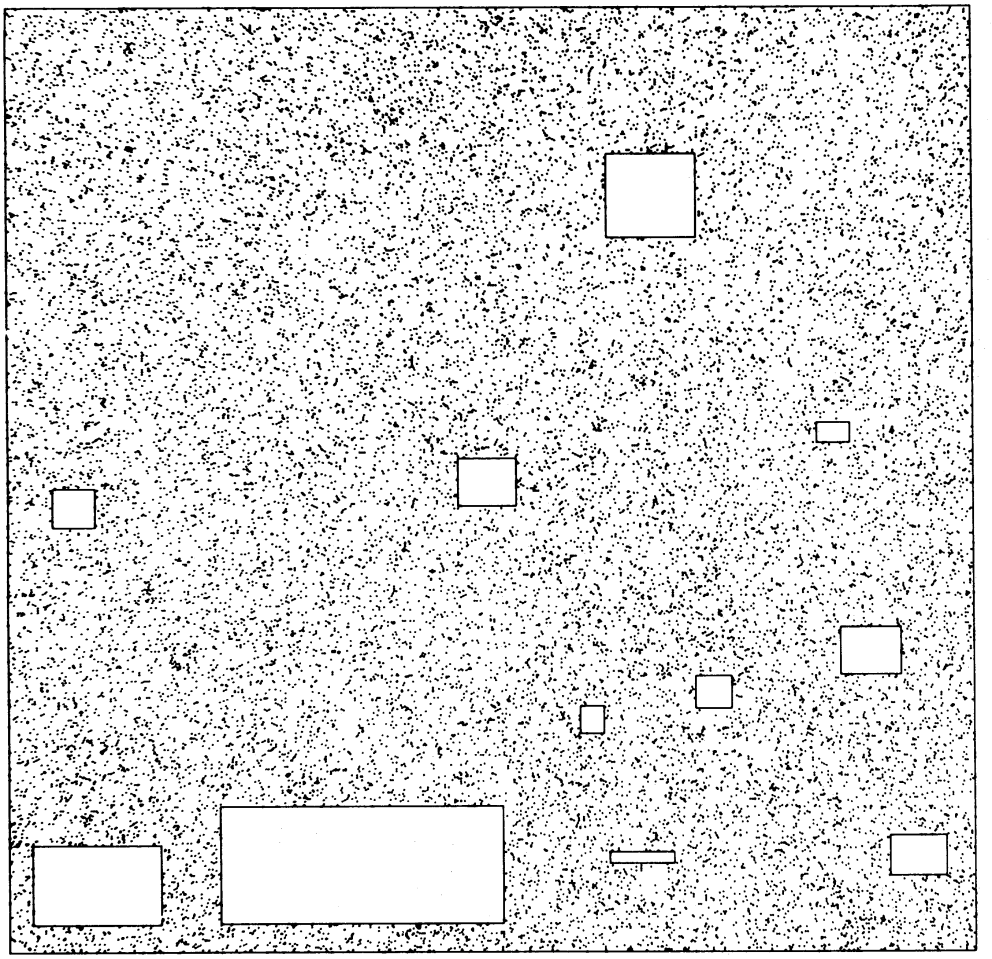

Figure 2(b)

3.2 UNFILTERED RESULTS

Using these estimators we obtain the correlation function given in Fig. 5 for the five plates. Although the estimates agree at small angles they differ markedly for $\theta > 0.3^\circ$. In this region the correlation functions show a change to steeper slope for the pair J3721/R2775 and for J1916. However, the function here falls only slowly for the J–R pair J1920/R3780. The consistency of the J and R correlation functions for each field suggests that this difference is *not* an artefact of photographic or measurement faults on individual plates.

It might be argued that the difference is caused simply by statistical fluctuations in the distribution of galaxy clusters and therefore only provides evidence that our samples are not 'fair'. We believe that this explanation is most unlikely since the difference occurs at a scale of only 0.1 times the dimensions of the measured area.

Fig. 6 shows the galaxy distribution for plate J1920. It reveals a striking gap in the distribution of more than 3° in length and 0.5° in width stretching in a north-westerly direction. This deficiency will make other areas of the plate look overdense on large scales and hence raise $w(\theta)$. The gap can also be seen in the galaxy distribution on plate R3780, though, in this case it is less pronounced. In contrast the galaxy distribution on plate J3721 is relatively flat on the largest scales.

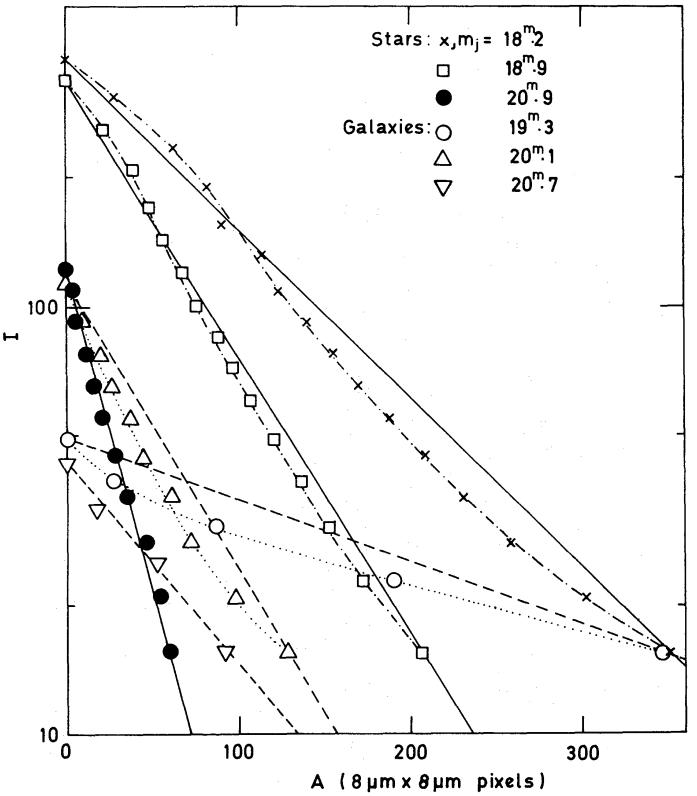

Figure 3. Profiles from COSMOS MM data of images on plate J1920 in terms of intensity, I (arbitrary units), as a function of area A. Straight lines are Gaussian fits to the central intensity and area at threshold. The isophotal magnitudes, obtained by pixel addition, differ from the Gaussian fitted isophotal magnitudes by only 0.01 mag for the 18.2 mag star and 0.14 mag for the 19.3 mag galaxy. As total magnitudes are used in the analysis, this difference is lessened by the obvious tendency of the Gaussian fit to underestimate the amount of light in the wings below the threshold.

To test whether an absorbing cloud may be responsible for this deficiency on the field of J1920/R3780, the extinction in the J and R passbands (A_J and A_R respectively) were calculated from number magnitude counts. Comparing counts inside and outside the gap we obtain $A_J = 0.25 \pm 0.05$ mag and $A_R = 0.12 \pm 0.05$ mag, consistent with reddening produced by interstellar dust (Allen 1973). If such an absorbing cloud does exist then the uniformity of the stellar distribution on this field suggests that it lies at some distance from the galactic disc. Efforts are now being made to obtain 21-cm observations which will hopefully clarify the origin of this interesting feature.

Thus there is some reason to believe that an effect not intrinsic to galaxy distribution is operating on the largest scales in the field of J1920/R3780. The best estimates of $w(\theta)$ are therefore, not given by Fig. 5, but by an estimator applied to the data after it has first been filtered to remove this induced large scale gradient.

3.3 FILTERED RESULTS

A 'moving average' filter was applied to the data by replacing the count in the i–jth bin, n_{ij}, by the smoother counts

$$n'_{ij} = \bar{n} n_{ij} / f_{ij} \qquad i, j = 1, \ldots 64. \tag{3}$$

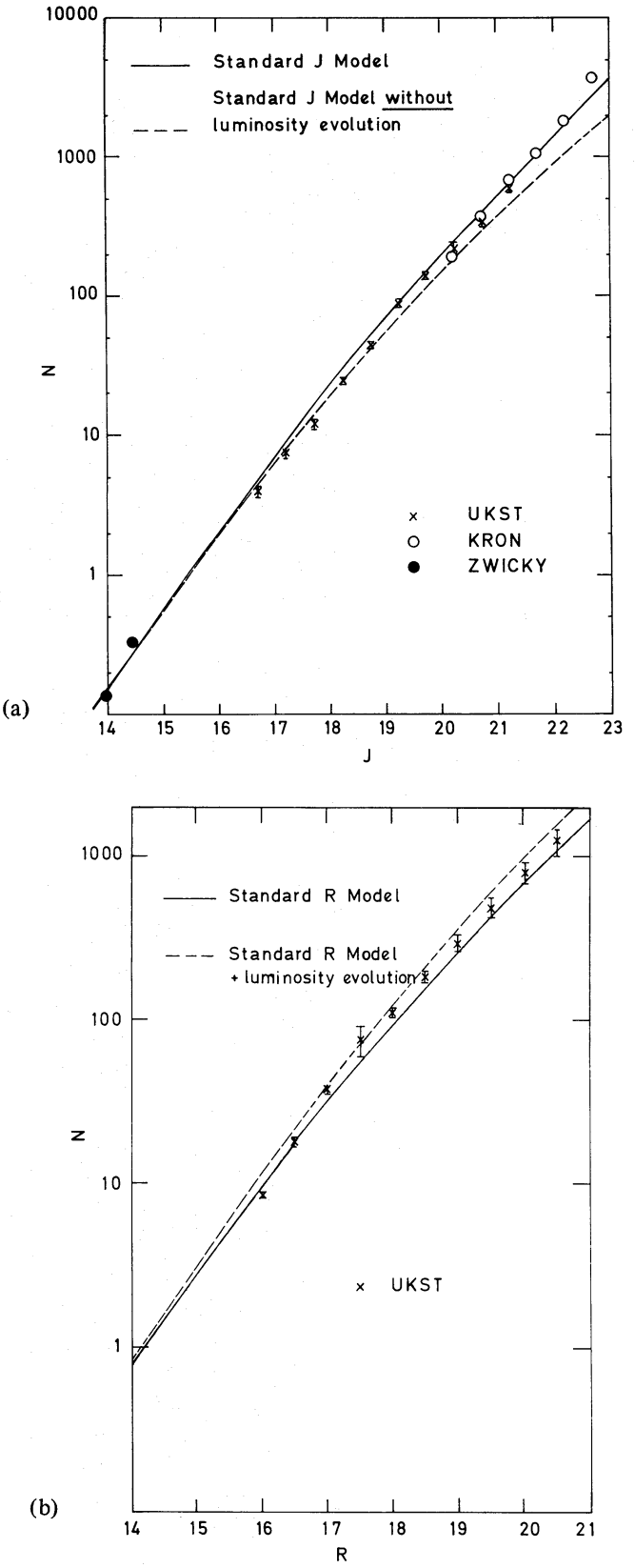

Figure 4. (a) Differential number counts per square degree for galaxies in 0.5 mag intervals plotted against J mag for various surveys. The UKST counts were taken from all three J plates. The solid curve is the prediction of the standard model. The dashed line has no luminosity evolution. The agreement between the UKST counts and other well calibrated data confirms the accuracy of our photometry. (b) As Fig. 4(a) but for R counts. The UKST counts were taken from both R plates.

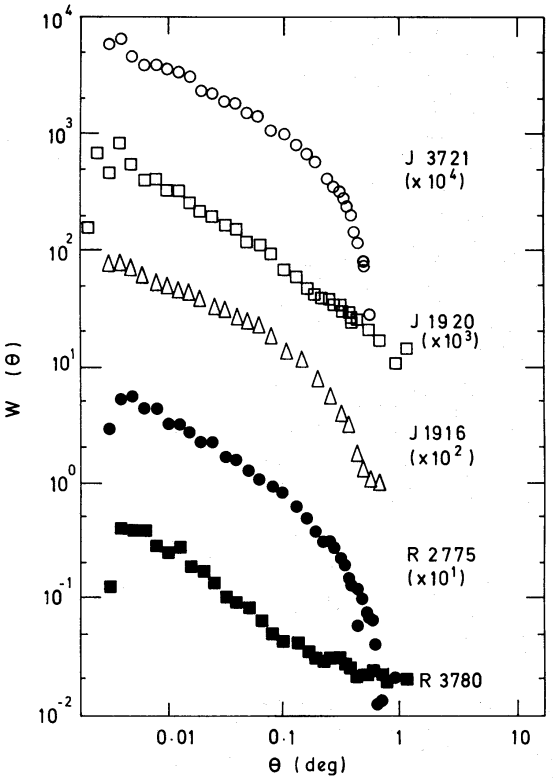

Figure 5. Unfiltered angular correlation functions for galaxies on the five plates listed in Table 1. The samples are limited at $J = 21.5$ and $R = 19.75$. The estimates are separated in the ordinate for clarity. Estimates of plates J1920 and R3780 (both field 412) show a different form to those for the other plates.

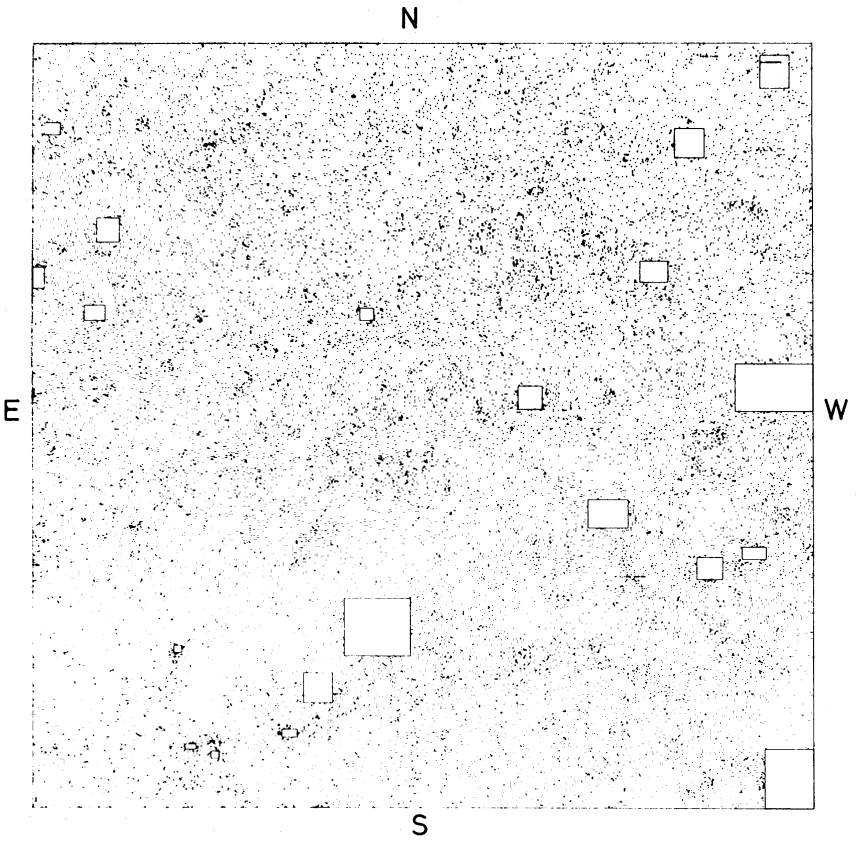

Figure 6. The distribution in position of galaxies for the sample limited at $J = 21.5$ on plate J1920. Notice the deficiency of images in a lane running in a north-westerly direction.

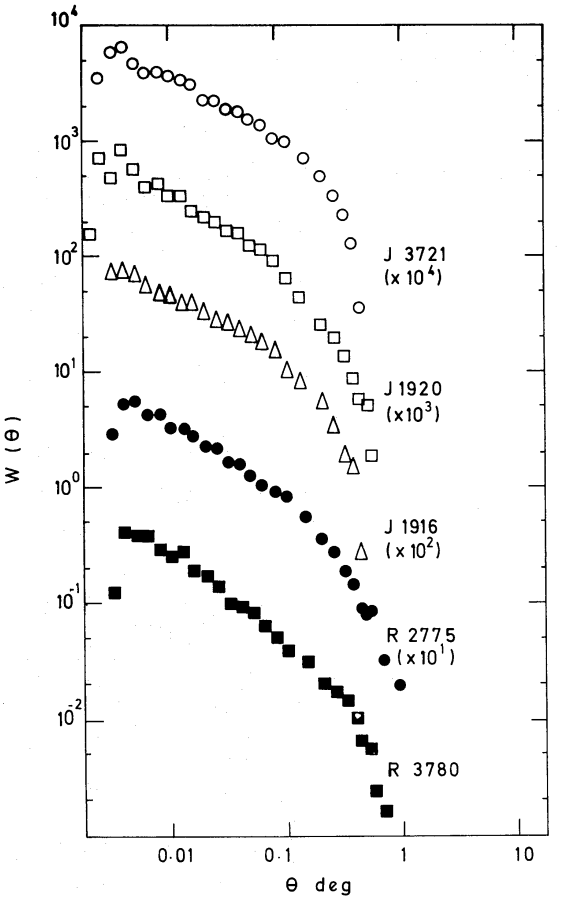

Figure 7. Filtered angular correlation functions for galaxies presented as in Fig. 5. Each estimate shows evidence for a feature at $\theta \sim 0.3°$.

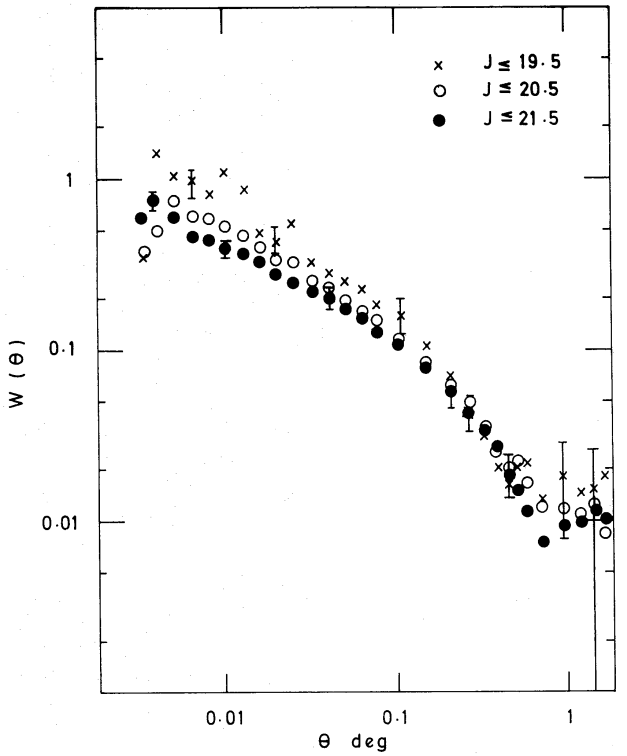

Figure 8. Unfiltered ensemble-averaged angular correlation functions limited at various magnitudes for the three *J* plates. Typical empirically-determined error bars are displayed.

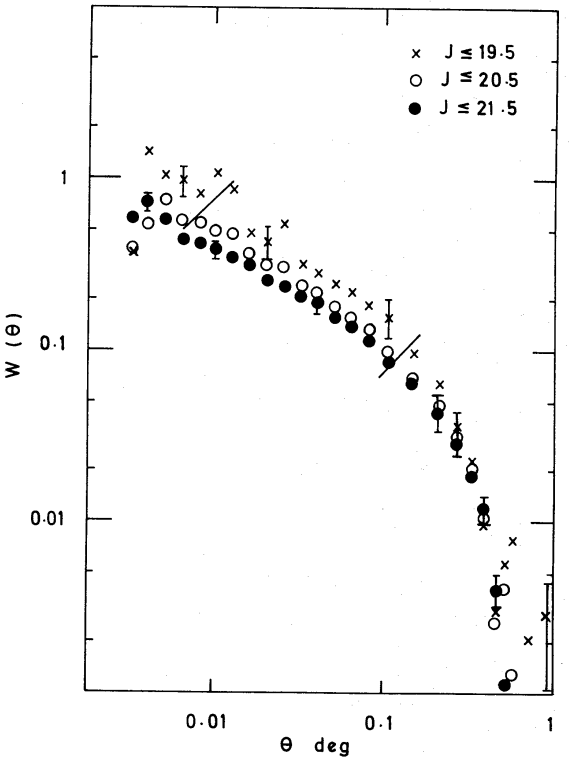

(a)

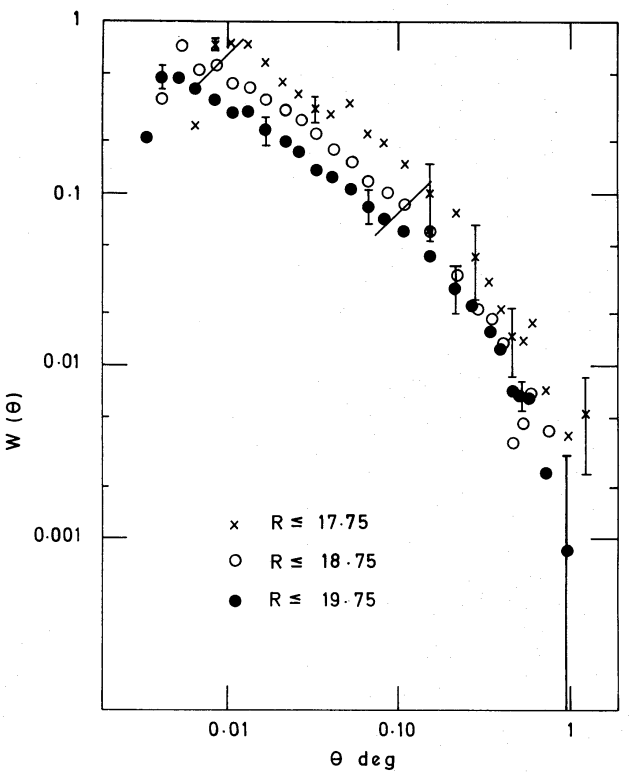

(b)

Figure 9. (a) Filtered ensemble-averaged angular correlation functions at various limiting magnitudes for three J plates. The solid lines show the range over which power-laws were fitted for the scaling comparisons. (b) As (a) but for the R plates.

Here, $\bar{n}$ is the average count per bin over the entire area and f_{ij} is the average count per bin in the occupied area within the immediately surrounding 32×32 bins (i.e. $1.9^\circ \times 1.9^\circ$ area). The filter width ($1.9^\circ \times 1.9^\circ$) was chosen to be sufficiently large to only smooth out density inhomogeneities the size of that discussed in Section 3.2 and larger. At the field edges f_{ij} is calculated for only those bins inside the measured field. The estimator of equation (2) is then applied using n_{ij}. For small θ the same f_{ij} is used, except that in this case, $\bar{n}/f_{ij}$ weights each *point* before applying equation (1).

Fig. 7 shows the filtered estimates for $w(\theta)$. At small scales there is little change from the unfiltered results for any of the plates. As expected, the estimate for J3721 is unchanged even at large scales. However, the new estimates for J1920 and R3780 now correspond well with those from the other two fields.

The appearance of a change in slope at the same scale length as that seen on the other two fields is not forced by the action of filtering. In numerous 2-D simulations the procedure has been shown to have negligible effect on $w(\theta)$ at scales less than 1.5° (Shanks 1979a). These simulations show that the correct analytical correlation functions for cluster models with randomly placed centres and diameters of $\sim 1^\circ$ were returned to good accuracy by the above filtering procedure even when strong large-scale gradients were present.

Thus it appears that $w(\theta)$ is similar for $0.005^\circ \lesssim \theta \lesssim 1^\circ$ on all five plates of three different fields. This, of course, does not preclude the possibility that some subtle systematic effect is conspiring to produce a common behaviour. The fact, however, that unfiltered results from J–R plate pairs of the same field give consistent results shows that if any such systematic effects are present, they do not dominate out estimates. Finally, it is worth noting that the same correlation results were obtained from the independently reduced MM data for J3721.

In Fig. 8 we show the ensemble averaged *unfiltered* correlation functions for the three J plates cut at limiting magnitudes of 19.5, 20.5 and 21.5. Their filtered counterparts are shown in Fig. 9(a). The similarity between the two sets is because the filtering is only necessary for one field. Fig. 9(b) shows the ensemble averaged correlation functions for the two R plates at limiting magnitudes of 17.75, 18.75 and 19.75. Empirically determined error bars are given where appropriate.

4 Scaling theory

4.1 PROJECTION EFFECTS

Comparisons between angular correlation functions obtained at different depths are called 'scaling tests'. In Paper I a scaling relationship between shallow and deep samples was obtained from a relativistic generalization of Limber's formula (Limber 1953) and was applied in the special case when the spatial correlation function $\xi(r)$ is a power-law in separation r. This relationship, which effectively accounts for projection and other geometrical effects, depends only on the sample selection function, $\phi(z)$, which is the probability of detecting a galaxy for the sample at redshift z. ϕ is determined in a manner independent of the galaxy angular positions by fitting models to the observed number–magnitude or number–angular diameter counts (see EFP). The scaling test is then used:

(a) as a test on the contamination of $w(\theta)$ estimates by galactic obscuration;
(b) as a test on the uniqueness of ξ over large volumes of space in an expanding Universe;
(c) as a test for evolution in ξ over the look-back time of deep samples.

4.2 DETERMINING THE SELECTION FUNCTION

In Paper I the deep samples were limited in surface brightness and angular size. In EFP the selection of galaxies by redshift was examined using the angular diameter counts. Obtaining the selection function for magnitude limited samples is more straightforward than for samples defined by surface brightness and size. It is important to verify, however, that our samples are genuinely magnitude-limited and not affected by the COSMOS detection cut-off. Fig. 10 shows that a number–magnitude prediction incorporating the cut-off at the appropriate isophote differs little from a prediction for a simple magnitude-limited sample. Furthermore, the data in Fig. 4 shows no fall-off in the observed number magnitude counts up to our deepest limits ($J = 21.5$ and $R = 19.75$).

The basic astronomical parameters governing the determination of $\phi(z)$ are the galaxy luminosity function (its shape, extent, normalization and mix with respect to morphological type), K-corrections and luminosity evolution and, finally, galactic absorption. Cosmological parameters have negligible effects over these depths. Table 3 gives the standard set of parameters used in the scaling calculations. The galaxy mix is taken from Pence (1976) and reproduces the observed mix at $m_B = 14.5$. This mix predicts a number–magnitude relation for the J band which is flatter than the observations (reproduced in Fig. 4a). The inclusion of Tinsley's (1978) slow star formation (SSF) evolutionary model is used to improve the fit, but this combination of mix and evolution is only one of many that fits the data. As Peterson *et al.* (1979) have shown, a mix more heavily weighted towards late types requires

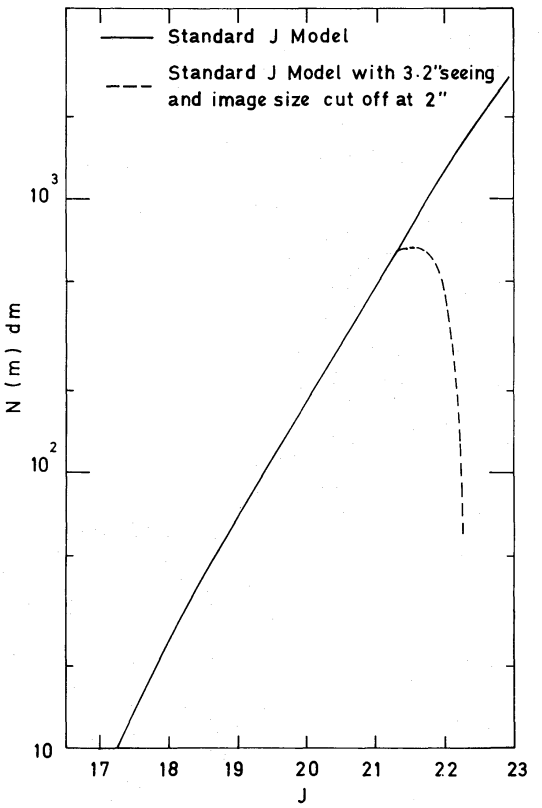

Figure 10. Predicted differential number magnitude counts for galaxies in the J band. The dashed curve applies to a sample defined by the COSMOS image size limit at the $\mu_J = 26.0$ mag arcsec^{-2} isophote. The solid curve applies to a deep sample unaffected by such size and surface brightness selection effects. Both predictions use the standard model. The agreement for $J < 21.5$ indicates the COSMOS selection procedure does not bias our magnitude limited samples.

Table 3. Standard astronomical parameters.

Galaxy type	Proportion (per cent)	M_J^*	α	$J-R$	$K_J(z)$	$K_R(z)$
E	12.5	−20.70	1.25	1.35	$5.0z - 1.4z^2$	$1.09z + 1.28z^2$
S0	25	−20.70	1.25	1.35	$5.0z - 1.4z^2$	$1.09z + 1.28z^2$
Sab	25	−20.80	1.25	1.15	$4.0z - 1.5z^2$	$1.02z + 0.92z^2$
Sbc	17.5	−20.95	1.25	0.80	$3.2z - 1.4z^2$	$-0.03z + 1.23z^2$
Scd	13	−20.30	2.00	0.66	$3.0z - 2.0z^2$	$-0.21z + 1.11z^2$
Sdm	7	−20.35	2.00	0.55	$2.0z - 1.5z^2$	$-0.63z + 1.03z^2$

Notes:

1. All data assumes $H_0 = 50$ km s^{-1} Mpc^{-1}.
2. Luminosity functions follow Schechter's (1976) relations with faint end slope α (see EFP equations 3 and 4), $\beta = 0.025$.
3. K-terms as a function of redshift z, $K(z)$, were calculated using data taken from Pence (1976).
4. Galactic absorption $A_J = 0.25$ mag, $A_R = 0.16$ mag was assumed.
5. Felten's (1977) normalization of $\Phi^* = 0.0022$ was taken for the luminosity function overall. This normalization applies outside the Galactic Poles, i.e. before any absorption correction.
6. Evolutionary corrections for the standard model were derived from the slow star formation models of Tinsley (1978).

virtually no luminosity evolution. The dilemma has been reviewed by Ellis (1979). Our inability to distinguish between the various combinations is not important for our scaling calculations. They require an average *effective* K-correction plus evolutionary term which is consistent with the observed number–magnitude counts; we shall adopt as the standard J model that defined by the Pence galaxy mix using Tinsley's SSF evolution. The K-corrections are derived as in Paper I, from tables in Pence (1976).

In the R passband we only have the COSMOS number–magnitude counts (Fig. 4b). The slope of the counts is consistent with Pence's mix and *no* luminosity evolution, although SSF evolution has a small effect in R and cannot be excluded. We adopt the no evolution model as the standard for the R passband. By comparing the counts with model predictions that utilize the observed colour indices of local galaxies to transform the J luminosity function into one in the R band, we obtain a night sky brightness $\mu_R^{\rm sky} = 21.75$ mag arcsec^{-2}, consistent with that obtained using Hawkins' sequences.

From these models selection functions are calculated and inserted in Limber's equation, as in Paper I, to give the expected amplitude of $w(\theta)$ at various limiting magnitudes.

5 Small scale clustering

5.1 POWER-LAW FITS

It is important to compare correlations for the different samples in a consistent manner. This is difficult because, although power-laws always give reasonable fits to our results, the index of the best fitting power-law is not always that obtained for shallow samples. To enable comparisons via Limber's formula, we fitted a -0.8 power-law at each depth over a fixed range of *spatial* separations. The spatial distances were calculated from the angular separations by assuming an effective angular diameter distance for each sample. The fitted range is indicated in Fig. 9. The correlations at small angular separations should not be affected by machine problems since, even for the $J < 19.5$ sample, 95 per cent of the

Table 4. Correlation amplitudes.

Sample	N	$A(\delta = 0.8)$ (corrected)	δ	B
J				
$M_J < 19.5$	182.2 ± 1.5	$(2.89 \pm 0.467) \times 10^{-2}$	-0.73 ± 0.076	1.41×10^{-2}
$M_J < 20.5$	530.9 ± 17.9	$(1.88 \pm 0.213) \times 10^{-2}$	-0.67 ± 0.023	5.71×10^{-2}
$M_J < 21.5$	1478.3 ± 83.9	$(1.50 \pm 0.166) \times 10^{-2}$	-0.57 ± 0.025	8.24×10^{-2}
R				
$M_R < 17.75$	146.5 ± 20.5	$(2.93 \pm 1.28) \times 10^{-2}$	-0.69 ± 0.06	1.01×10^{-2}
$M_R < 18.75$	439.5 ± 34.5	$(1.69 \pm 0.433) \times 10^{-2}$	-0.73 ± 0.022	8.0×10^{-2}
$M_R < 19.75$	1225.0 ± 125.0	$(1.09 \pm 0.202) \times 10^{-2}$	-0.69 ± 0.020	4.26×10^{-2}

Notes:

The fits were done between the lines shown in Fig. 9. The errors quoted for δ are least-squares errors of fit. All other errors were empirically determined by averaging between plates.
The amplitude A has been corrected upwards by a factor of 1.23 to account for 10 per cent contamination of the galaxy samples by stars during automatic star–galaxy separation.
N is the number of galaxies per square degree.

galaxies have an isophotal angular diameter less than the lower θ limit. The large θ limit is carefully placed so as to avoid any problems with the steepening of $w(\theta)$ at large scales.

Table 4 gives the best fitting amplitudes A for the form

$$w(\theta) = A\theta^{-0.8}. \tag{4}$$

A was fitted using log–log least-squares techniques. The best fitting power-law indices δ, and their corresponding amplitudes B for the more general form

$$w(\theta) = B\theta^{-\delta} \tag{5}$$

are also given in the table. These were also fitted using a log–log least-squares procedure. In most cases we give the empirically estimated standard errors found from averaging the individual fits to each curve making up the ensemble.

Finally in Table 4 amplitudes are also corrected for contamination by stars due to the identification errors that must exist in any form of star–galaxy separation. Our stellar samples are effectively randomly distributed on all scales greater than the limit to which the power-laws were fitted. If w is the observed correlation function for a sample composed of fractions f_g and f_s for galaxies and stars respectively, then

$$w = f_g^2 w_{gg} + f_s^2 w_{ss} \tag{6}$$

where w_{gg} refers to the true galaxy correlation function and w_{ss} to that for the accidentally included stars. (We assume no cross-correlation between stars and galaxies.) Eyeball checks show that f_g and f_s are about 0.9 and 0.1 respectively for all our samples. Thus if $w_{ss} \equiv 0$ for all θ in our range, $w_{gg} = w/0.81$ and the true amplitude is higher by 23 per cent.

5.2 SCALING COMPARISONS

The corrected amplitudes for the J and R ensembles are plotted together with the predictions in Fig. 11. The amplitudes measured by Peebles and co-workers for the shallow catalogues are also shown.

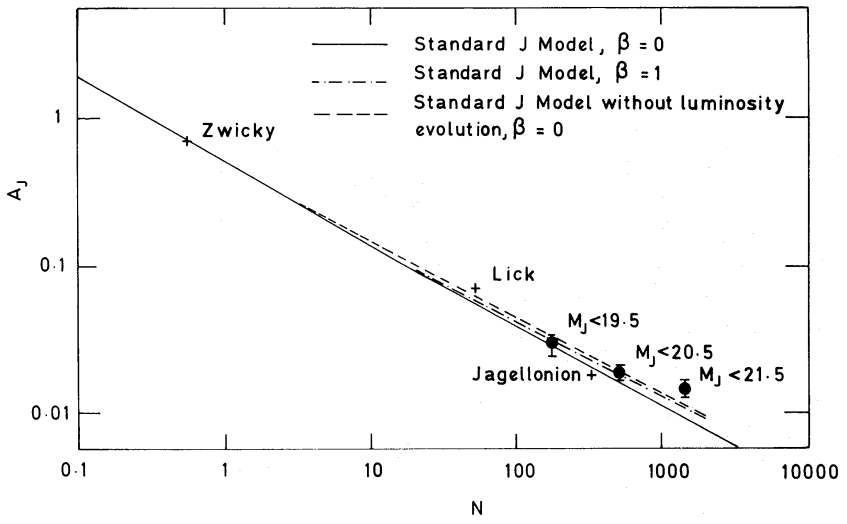

(a)

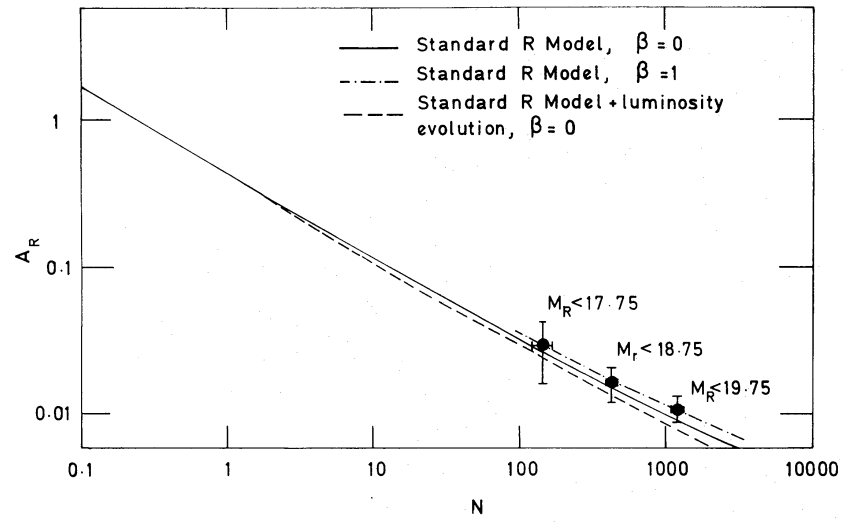

(b)

Figure 11. (a) Amplitudes of -0.8 power-law fits to the galaxy angular correlation function plotted against galaxy surface density per square degree. The corrected observed amplitudes are to be compared with model predictions allowing for geometrical and projection factors. The solid curve uses the standard model. The dashed curve shows the effect of excluding luminosity evolution. The dot–dash curve allows clusters to be fixed in comoving space rather than in proper space ($\beta = 1$ not 0 in the notation of Paper I). (b) As (a) but for the R band.

The scaling behaviour of the deep samples agrees well with the predictions of the standard models described in Section 4.2; there is no large discrepancy such as that found for the samples of Paper I. With the exception of the deepest J cut, the amplitudes agree with the predictions of the standard models to an accuracy of better than 20 per cent which is well within the indicated errors. (See Section 5.4 for a discussion of the results for the $m_J < 21.5$ sample.) Thus these amplitudes scale to the Zwicky amplitude as well as those amplitudes obtained from the SW and Jagellonian samples. This is an encouraging result in support of the basic cosmological assumptions of the homogeneity and isotropy of the Universe on very large scales. It indicates that the same model of galaxy clustering is applicable out to a luminosity distance of $\sim 700\ h^{-1}$ Mpc. It is also encouraging to note that

the standard parameters (Table 3) used to fit the galaxy number–magnitude counts reasonably explain the deep-angle correlation functions. The two tests are not identical, for the scaling relations depend critically on the shape of $\phi(z)$ being particularly sensitive to changes in K-corrections and luminosity evolution.

5.3 THE OBSERVED SLOPES

Table 3 shows that the best power-law index (equation 5) is sometimes substantially flatter than the value -0.77 ± 0.05 quoted by Peebles (1974) for the local samples. The R plates and the shallowest J samples give a mean $\delta = -0.71 \pm 0.012$, which is reasonably consistent with the local value. The indices for the deeper J samples, however, appear to become flatter with increasing depth. A possible systematic machine effect is unlikely as only the J samples are affected.

A ready explanation of this phenomenon is provided by the preferential selection of spirals as the J samples reach fainter; the E/S0 K-correction in J is much greater than for spirals. Thus, considering that E/S0's are more highly clustered than spirals, the observed flattening is not surprising. We have further checked using the approximate correlation results of Davis & Geller (1976) for the different morphological types that the scaling carried out above is not seriously affected by this selection effect.

For the R passband, the difference between the K-corrections for E/S0's and for spirals is much less and, as observed, would then have little effect on the power-law index. A more detailed discussion will be given in a subsequent paper, in which colour subsamples of the present data are analysed.

5.4 DISCUSSION

The scaling discrepancy of Paper I cannot be explained by contamination of the samples by stars, as f_s would then have to be ~ 0.4 (equation 6). The discrepancy was thought to be due to the small areas covered (≈ 2 deg^2), i.e. sampling problems. The amplitudes obtained by dividing plate J3721 of this sample into four areas of comparable depth and size gave a standard error of ± 20 per cent in the fitted amplitude, which does indeed indicate that 2 deg^2 at these depths might not provide a fair sample for small-scale clustering analyses.

However, although the field in Paper I could well be a rather special one, an additional explanation for the discrepancy may be that the photometry of the faintest images for those samples was much more inaccurate than for the present COSMOS runs.

In Paper I the smallest images would frequently consist of only ≈ 15 pixels (*cf.* 50 pixels here). Although the EFP models showed such samples were reasonably well-defined, the models could not allow for the effects of random errors both in the COSMOS measurements and in the emulsion on the plates themselves. Fluctuations in image size at the limit could be so large as to contaminate the sample with images actually much fainter than the supposed limit, thus broadening $\phi(z)$ and lowering the correlations.

This explanation is supported by experiments with COSMOS where the effective number of pixels per image was reduced. Discrepant correlation amplitudes (to factors ~ 2) were obtained at the faintest limits where previously the data had scaled reasonably accurately. And, indeed, Paper I did show a reduction in the discrepancy when analysis was confined to larger images.

As has been noted, the deepest J sample $w(\theta)$ amplitude does not scale as well as the amplitudes from the other five samples. The amplitude here is some 50 per cent *higher* than is predicted with the standard J model. The size of the correlations being *larger* than

predicted is slightly disturbing since, as we have seen, most errors tend to diminish the correlations. However, if we have overestimated the amount of star contamination in this particular sample then simply by omitting the corresponding correction factor we find that this deep result lies within one standard error of the prediction. Therefore, since the errors on the amplitudes may be larger than those indicated in Fig. 11 because of such systematic effects, we shall not, at present, attach too much significance to this result.

A detailed interpretation of the present scaling results is difficult because the errors are often as large as the effects we might reasonably expect to detect. Nevertheless, it is worth noting the effect of varying some of the standard parameters on the fits to the observed amplitudes in Fig. 11. Removing SSF luminosity evolution from the J standard model improves the fit to the J sample amplitudes (but, of course, produces a less good fit to the number counts of Fig. 4). The R amplitudes seem to prefer very little luminosity evolution in agreement with the rough indications from the COSMOS R number counts. We note finally, that it is possible to further improve the model agreement in both J and R by introducing correlation evolution. This is done by putting $\beta = 1$ in the prediction for the standard model (see Paper I and Fig. 11), but clearly such a detailed discussion must await machine measured data to fainter limits (a) to better define the galaxy number magnitude relations and hence the 'effective' galaxy K-correlations and (b) to determine any evolutionary trends over a wider range in limiting magnitudes.

6 Large scale clustering

6.1 INTRODUCTION

The possible existence of a feature in the galaxy correlation function at large angular scales (Groth & Peebles 1977) is an exciting prospect for theories of galaxy formation, since it may define a characteristic scale of clustering. It is therefore, very important to establish whether this feature is *real,* that is, produced by true spatial clustering, or whether it results from systematic selection effects operating in the SW catalogue (although Groth & Peebles give arguments against this latter possibility). In the long term, it may be possible to obtain $\xi(r)$ directly by analysing complete redshift catalogues (Kirshner, Oemler & Schechter 1979). However, present redshift samples are too small to allow an unequivocal estimate of $\xi(r)$ to be made at the scales of interest.

6.2 SCALING COMPARISONS AT LARGE SCALES

For the samples presented here, Table 4 shows that at small scales the correlation estimates are well represented by a power-law of index ~ -0.7 or shallower. At larger angles, however, they break sharply away from the power-law (see Fig. 9a and b) and there are no $w(\theta)$ points significantly above zero after $\sim 0.5^\circ$. Indeed, points at $\theta > 0.3^\circ$ would have to be raised by over 5σ to maintain the power-law fits.

This break is not produced by the integral constraint applying because we have estimated the average number density and $w(\theta)$ from the same area. A maximum difference of 0.01 is caused in the $w(\theta)$ for the $M_J < 21.5$ samples by using, instead, an ensemble average number density in the estimator of w. The addition of this amount to $w(\theta)$ has little effect and thus the feature has not been produced in this way. Neither can the break be explained as being due to contamination by a randomly distributed population of stars for the shape of $w(\theta)$ would still be maintained (see equation 6).

The crucial test of the reality of this feature is to check whether it scales correctly with depth. To perform the scaling test we adopt the method of Groth & Peebles (1977), where a

Table 5. Scaling factors for the feature.

J samples	x	y	$h D^*_{\rm eff}$ (Mpc)
19.5	0.920	0.780	336.1
20.5	0.888	0.721	479.5
21.5	0.853	0.665	668.7
R samples			
17.75	1.020	0.934	300.0
18.75	0.984	0.856	432.6
19.75	0.937	0.768	608.9

two power-law model is inserted in the relativistic version of Limber's formula. We choose the indices to be -1.8 and -2.8, but the required factors are insensitive to reasonable variations in these indices. Table 5 gives the values of the scaling factors x, y and $D^*_{\rm eff}$ at our various depths. These factors are defined exactly as in Groth & Peebles. To allow a fair comparison of the *large scale* behaviour of $w(\theta)$ we chose the parameters from Fig. 11 which best described the small angle scaling behaviour. Since these do not adequately describe the small angle scaling result for the $M_J < 21.5$ sample, we have not used this sample in the diagrams that follow.

The results of scaling Fig. 9 via Table 5 to the Zwicky depth are shown in Fig. 12(a). The scaling behaviour at large angle is seen to be less consistent than at small angles showing

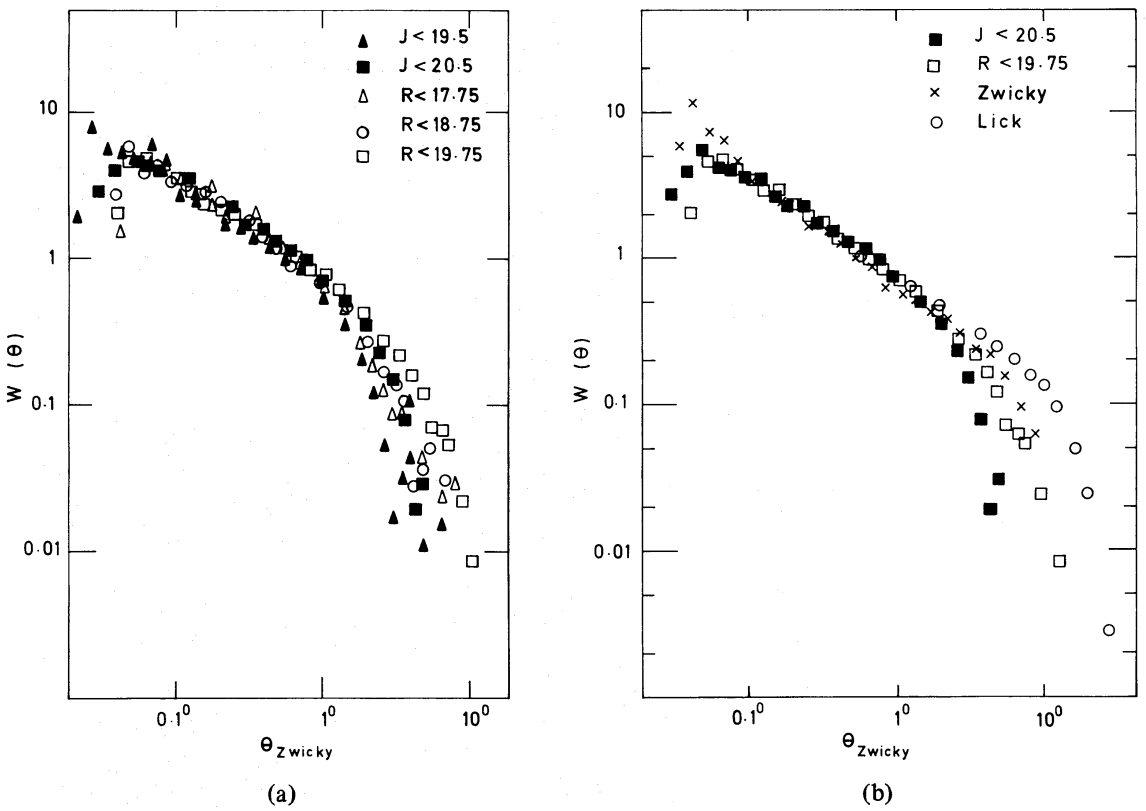

Figure 12. (a) Angular correlation functions for the ensemble-averaged samples scaled to the depth of the Zwicky catalogue. (b) Angular correlation functions for the deepest samples of (a) together with the Zwicky and scaled Shane–Wirtanen results. The feature in the UKST samples occur at smaller separations.

some slight systematic effects as the samples go deeper. However, in view of the uncertainties in the estimation we regard the scaling agreement shown in Fig. 12(a) as remarkably good. In Fig. 12(b) the deepest J and R cuts from Fig. 12(a) are reproduced along with the results from the Zwicky catalogue and the scaled SW counts (as estimated by Groth & Peebles). Although the agreement at large scales between the Zwicky catalogue and the deep samples is reasonable, the agreement is not so good with the SW results. The feature in the SW results occurs at $\theta_{\text{Zwicky}} = 10^\circ$ whereas in our sample it occurs at $\theta_{\text{Zwicky}} = 3^\circ$. Thus our estimate corresponds to a break in ξ at around 3 h^{-1} Mpc instead of at 9 h^{-1} Mpc. Since this discrepancy persists even in our shallowest sample whose limit is within 1 mag of the SW limit, the difference cannot be resolved by a judicious choice of any parameter in the scaling procedure.

Before discussing these results further we now demonstrate that there is no bias in our $w(\theta)$ estimators which artificially creates or moves the feature by showing that an independent statistical analysis, Mead's analysis, corroborates our large-scale correlation estimates.

6.3 MEAD'S ANALYSIS

Mead's Analysis is described in detail by Shanks (1979b) and references therein. Briefly, a statistic $S(\theta)$, designed to reveal the angular size of any preferred scale in the galaxy clustering, is calculated. The statistic has the advantage that small θ estimates are *unaffected* by large scale number density gradients in the data. Thus, no filtering ambiguities are encountered. Now, if we were to interpret the feature discussed above to be the scale-length of a preferred cluster size seen at an average distance for our sample, then we should also expect to see a peak in the $S(\theta)$ statistic at the appropriate angle.

The Mead's Analysis of the $J < 21.5$ ensemble is shown in Fig. 13. The $S(\theta)$ statistic clearly peaks in the region $0.12^\circ - 0.24^\circ$ and falls sharply away for scales greater than the $w(\theta)$ break point of 0.3°. (The peak in $S(\theta)$ occurring slightly shortwards of the maximum clustering size, is expected on the basis of application of Mead's analyses to simulated galaxy distributions – see Shanks 1979a.) Furthermore, $S(\theta)$ behaves no differently on J1920, the field we had to filter, than on J3721. The analysis, therefore, gives very convincing evidence in support of the reality of the feature. The small-scale behaviour of $S(\theta)$ also gives further support to the contention that the correlation statistics are more consistent with galaxies being distributed in clusters with power-law density fall-offs than in a hierarchical pattern (Shanks 1979b).

6.4 DISCUSSION

Although we have shown Section 5 that our small-scale $w(\theta)$ estimates are consistent with those expected from shallower catalogues, there is now some discrepancy between the large scale behaviour of the deep samples and that of the SW counts. We have discussed carefully sources of possible error in our estimates. These include the possibilities that:

(a) our sample is not a 'fair' one on large scales (see Section 3.2);

(b) the filtering of J1920/R3780 has biased the results (see Sections 3.3 and 6.3);

(c) there is a 'sample size' bias in our estimator of $w(\theta)$ on all the plates (see Section 6.3);

(d) some systematic error has been introduced into our galaxy distribution during, say, star–galaxy separation (see Section 2).

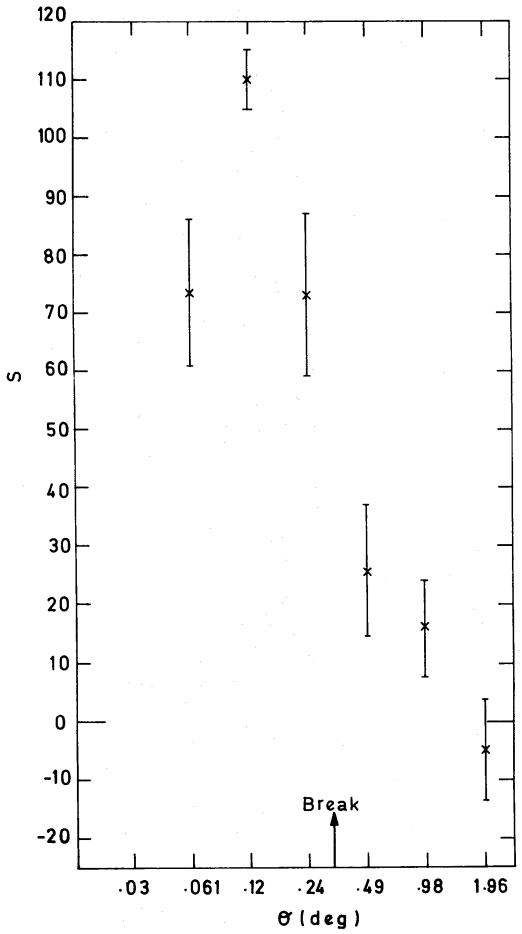

Figure 13. Mead's Analysis of the ensemble-averaged sample limited at $J = 21.5$. The ordinate represents the degree of clustering at various angular separations. The peak in the statistic occurs at approximately the angle corresponding to the feature observed in the correlation function.

Arguments have been given against all these explanations and these become stronger when taken together with the fact that our samples scale reasonably well with respect to one another, and also by the fact that the filtered results are reproducible from one plate to another. If there is an error, we consider (d) to be the most likely source, since such effects are the most difficult to detect.

On the other hand, there are also serious difficulties in estimating the position of the feature on the shallower surveys. We have already mentioned the difficulties encountered with galactic obscuration. Although the feature is seen in the estimates for the Zwicky catalogue its position does not scale to better than a factor of ~ 2 to the SW feature (see Groth & Peebles 1977, Figs 13 and 14). Furthermore, the smoothing applied by Groth & Peebles to the SW counts would not remove the effects of emulsion or obscuration variations over a single plate. If such 'within-plate' effects were common, they would act like the obscuration on J1920, keeping the SW correlations artificially high. A good check on contamination by small scale obscuration will be to apply the Mead's Analysis to the SW counts.

Finally, although in this discussion we have emphasized the differences between our results and those of Groth & Peebles, it must not be forgotten that *both* analyses indicate the existence of a feature in $\xi(r)$. Considering the different methods of compiling the

catalogues with all the difficulties involved, the discrepancy in position, in experimental terms, may not be too serious.

7 Conclusions

We have seen from analyses of deep machine-measured samples of galaxies taken from five UKST plates of three fields around the South Galactic Pole that:

(i) the amplitude of the small scale galaxy correlations is in good agreement with that expected from the results of shallower surveys. This scaling was done assuming a galaxy luminosity function and an effective K-correction which were consistent also with galaxy number–magnitude counts presented here using COSMOS and from other sources. The scaling agreement is powerful evidence that the locally derived spatial correlation function is applicable to depths of $\sim 700\ h^{-1}$ Mpc;

(ii) on large angular scales the correlation functions show good evidence for a feature at separations corresponding to $3\ h^{-1}$ Mpc. Although the large angle correlations scale reasonably amongst our samples, this position is a factor of ~ 3 smaller than the feature found by Groth & Peebles (1977) in their analysis of the Shane–Wirtanen counts. However, considering the uncertainties involved such a discrepancy may not be too serious.

Acknowledgments

We gratefully thank the staff at the UK Schmidt telescope for cooperation and hospitality extended to RSE during the period when some of these plates were taken. We also acknowledge the perseverence and help of the Royal Observatory, Edinburgh, especially Drs R. D. Cannon, R. Martin and R. Stobie. Drs J. Graham, M. R. S. Hawkins, W. D. Pence and B. M. Tinsley are thanked for supplying material prior to publication. Drs D. Carter and J. Godwin are thanked for their assistance with the PDS measurements. Thanks are also due to Drs S. Phillipps, A. W. Strong and Mr G. Efstathiou for useful discussions. One of us (TS) was supported by the SRC during the period of this work.

References

Allen, C. W., 1973. *Astrophysical Quantities,* p. 264, Athlone Press, London.
Davis, M. & Geller, M. J., 1976. *Astrophys. J.,* **208**, 13.
Davis, M., Groth, E. J. & Peebles, P. J. E., 1977. *Astrophys. J.,* **212**, L107.
Efstathiou, G., 1979. *Mon. Not. R. astr. Soc.,* **187**, 117.
Ellis, R. S., 1979. *Phil. Trans. R. Soc. Lond.,* **A296**, 355.
Ellis, R. S., Fong, R. & Phillipps, S., 1977. *Mon. Not. R. astr. Soc.,* **181**, 163.
Fall, S. M., 1979. *Rev. mod. Phys.,* **51**, 21.
Felten, J. E., 1977. *Astr. J.,* **82**, 861.
Groth, E. J. & Peebles, P. J. E., 1977. *Astrophys. J.,* **217**, 385.
Kirshner, R. P., Oemler, A. & Schechter, P. L., 1979. *Astr. J.,* **84**, 951.
Kron, R. G., 1978. *PhD thesis,* University of California, Berkeley.
Limber, D. N., 1953. *Astrophys. J.,* **117**, 134.
MacGillivray, H. T. & Dodd, R. J., 1979. *Mon. Not. R. astr. Soc.,* **186**, 69.
MacGillivray, H. T., Martin, R., Pratt, N. M., Reddish, V. C., Seddon, H., Alexander, L. W. G., Walker, G. S. & Williams, P. R., 1976. *Mon. Not. R. astr. Soc.,* **176**, 265.
Malin, D. F., 1978. *Nature,* **276**, 591.
Oemler, A., 1974. *Astrophys. J.,* **194**, 1.
Peebles, P. J. E., 1974. *Astr. Astrophys.,* **32**, 197.
Pence, W., 1976. *Astrophys. J.,* **203**, 39.

Peterson, B. A., Ellis, R. S., Kibblewhite, E. J., Bridgeland, M. T., Hooley, T. & Horne, D., 1979. *Astrophys. J.*, **233**, L109.

Phillipps, S., Fong, R., Ellis, R. S., Fall, S. M. & MacGillivray, H. T., 1978. *Mon. Not. R. astr. Soc.*, **182**, 673.

Pratt, N. M., Martin, R., Alexander, L. W. G., Walker, G. S. & Williams, P. R., 1975. *Image Processing Techniques in Astronomy*, p. 217, D. Reidel, Dordrecht, Holland.

Schechter, P., 1976. *Astrophys. J.*, **203**, 297.

Shanks, T., 1979a. *PhD thesis*, University of Durham, England.

Shanks, T., 1979b. *Mon. Not. R. astr. Soc.*, **186**, 583.

Tinsley, B. M., 1978. *Astrophys. J.*, **220**, 816.